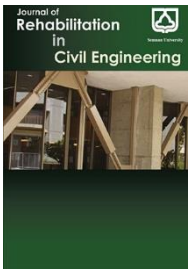

Journal homepage: http://civiljournal.semnan.ac.ir/

Investigating Cyclic and Pushover Performance of Different Metallic Yielding Dampers

Ali Mohammad Rousta[1*], Sohrab Shoja[2], Masoud Amin Safaei Ardakani[2]

1. Assistant Professor, Department of Civil Engineering, Yasouj University, Yasouj, Iran.
2. Graduate of M.Sc. Structural Engineering, Department of Civil Engineering, Yasouj University, Yasouj, Iran.
Corresponding author: *arousta@yu.ac.ir*

ARTICLE INFO

Article history:
Received: 12 April 2022
Revised: 25 August 2022
Accepted: 21 September 2022

Keywords:
Steel structures;
Metallic yielding dampers;
Passive devices;
Effective stiffness;
Effective damping.

ABSTRACT

One of the most widely used and applicable solutions for limiting the damages of earthquakes to steel structures is using Metallic Yielding Dampers as a type of passive devices to dissipate the received energy. Maintaining a proper balance in the design of these devices is a delicate matter as each of the different types have advantages and disadvantages. In this research, different types of metallic dampers are compared using finite element simulation which is performed by means of ABAQUS package. Modeling process is described and verified by comparing the results to a previously published experimental paper on the subject. For assuring more accuracy a mesh convergence analysis is performed to determine the suitable mesh size. Afterwards, cyclic and pushover analysis are performed on each damper and results are presented and discussed. Effective stiffness and damping of each damper, both general and average, is extracted using proper equations and finite element results. Finally, for deeper understanding of dampers behavior, internal forces of the dampers are derived and compared. It was shown that design equations are fairly accurate. As the height of the dampers increases, their effective stiffness and damping reduces and the dampers behavior leans towards flexural behavior. Based on cyclic and pushover analysis, Steel Plate Dampers (SPD) have the highest stiffness and energy dissipation. Also, SPD and Double Pipe Dampers (DPD) are the most suitable to reach a demanded stiffness, damping and have the most stable performance. At the end of the paper, a list of conclusions is presented.

How to cite this article:
Rousta, A. M., Shoja, S., & Amin Safaei Ardakani, M. (2023). Investigating Cyclic and Pushover Performance of Different Metallic Yielding Dampers. Journal of Rehabilitation in Civil Engineering, 11(3), 122-143.
https://doi.org/10.22075/JRCE.2022.26848.1639

1. Introduction

Achieving higher rotation capacity and ductility concurrent to maintaining highest possible rigidity in beam to column connections of steel structures is one of the most challenging problems in design process of steel buildings with moment resisting frames. This means, ductile rigid connections must have the ability to provide sufficient strength and rotation capacity at the same time [1]. Although steel moment resisting frame (MRF) structures are designed in a way that large inelastic deformations during earthquakes occur in the main structural members [2], the most significant issue in this type of connections is low rotation capacity compared to high resistance [1]. This causes sudden fracture at the junction of the beam flange to the column before the formation of a plastic joint in the beam [1].

Although many buildings were designed to withstand total collapse and as a result saved many lives during the Northridge (1994) and Kobe (1995) earthquakes [3,4], large number of steel structures became damaged in their structural members [5]. These damages were mostly concentrated on the beam to column welded connection, which was due to the brittle fracture of the welded joint [6]. After the mentioned earthquakes, many studies were conducted on beams with reduced cross-section [6, 7] and side plates [8] as the most widely accepted alternatives to former beam to column connection types. The mentioned elements maintain beam to column connection in the elastic state, until plastic joints, which are the main source to increase the energy dissipation capacity, are created in the beam [1, 9, 10]. Since seismic design of these connections is based on the rotation capacity of the joint, and after earthquakes happen the connection area is supposed to enter the plastic state, maintenance and restoration of such connections are not easily applicable or feasible [6]. Therefore, searching for alternative solutions, one of which is using damage-control equipment, is suggested to overcome this problem.

One of the most prevalent solutions is using Metallic Yielding Dampers (MYDs). These dampers use inelastic deformations to dissipate energy after reaching the yielding point [11]. Using these types of beam to column connections have many advantages such as stable hysteretic behavior, low sensitivity of connection to ambient temperature changes, high long-term reliability and low implementation cost. Steel Slit Dampers (SSD) were first introduced by Oh [12]. Various experimental and numerical studies on SSD dampers [1,6,12,13,14] show that these dampers provide suitable rotational behavior, high energy dissipation, efficient and economical implementation, and at the same time prevent major damages to the beams. However, there are two problems with the function of these dampers which are excessive shear in damper struts and also buckling of the damper struts [15,16], as shown in Figure 1, and as a result, possibility of brittle strut fracture.

In order to eliminate these problems, in addition to increasing stiffness of these dampers, these devices were improved by changing the shape and configuration. These changes improved SSDs behavior against imposed stresses, by reducing the simultaneous effect of bending and shear stress. In this regard, Metallic Yielding Dampers (MYDs) with other shapes and configurations were presented and studied by many researchers [17-21].

In addition, hybrid dampers are presented in different combination and configurations by many researchers in recent years [22-25].

a. buckling of the damper legs model examined by Ma et al. [26].

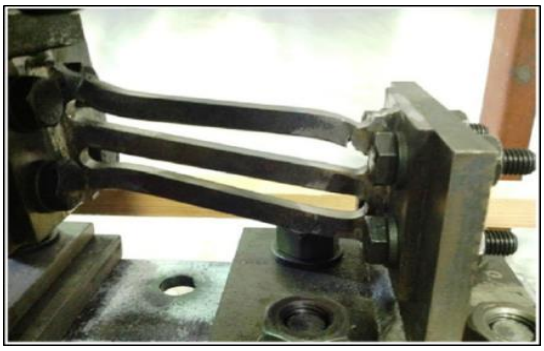

b. buckling of the damper legs model examined by Tagawa et al. [27].

c. buckling of the damper legs model examined by Lee et al. [28].

Fig 1. The buckling of SSD damper legs.

Although, this is only a part of the studies conducted on Metallic Yielding Dampers, the vast number of studies shows the practicality and demand of Metallic Yielding Dampers performance improvement against seismic loadings. Therefore, different dampers with different shapes and behavior, each of which had its advantages and disadvantages compared to previous ones, were presented by researchers. Steel Plate Added Damping and Stiffness Elements (ADAS) [29], Dual-Pipe Damper (DPD) [30], Shear-and-Flexural Yielding Metallic Dampers (SAFYD) [31], Steel Panel Damper (SPD), Steel Slit Damper (SSD) and Steel Shear Panel Dampers (SSPD) [32], are in this category. However, structural engineers are always faced with the difficulty of choosing one type of structural system over another. Metallic Yielding Dampers are no exception in this regard and there are not many researches comparing different MYDs at the same time. Since there are many types of these systems, comparing different types simultaneously, from several aspect and perspective, will give the designers the benefit of having enough information on how these dampers behave and help them reach a conclusion based on their structures' demand.

2. Introduction and Confirmation of Materials Behavior

The numerical analysis in this research has been conducted with the powerful ABAQUS package [33]. The material used in the modeling process is ST37 which is a structural mild steel with a yield stress equal

to 241 MPa. Mechanical characteristics of ST37 steel are presented in Table 1. For modeling the steel, three linear behavior with combined plastic hardening is considered. The article by H. A. Amiri et al. [35] on Block Slit Damper has been used to verify and confirm the behavior of materials and the modeling process. Geometrical characteristics of the models and the loading protocol used by Amiri et al. are shown in Figure 2 and Table 2.

Table 1. Mechanical characteristics of ST37 steel [34].

Steel Material	Modulus of elasticity (MPa)	Yield Stress (MPa)	Ultimate Stress (MPa)	Elongation (%)
ST37	200	241	403	29.8

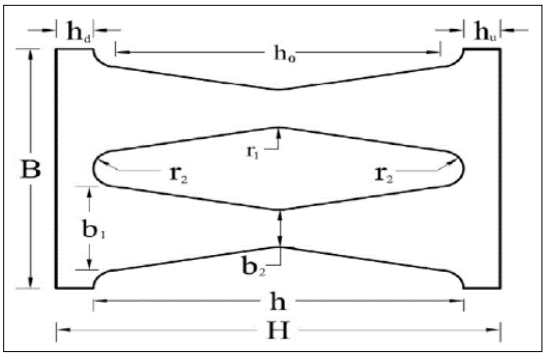

a. Geometrical parameters of specimens studied by Amiri et al. [34].

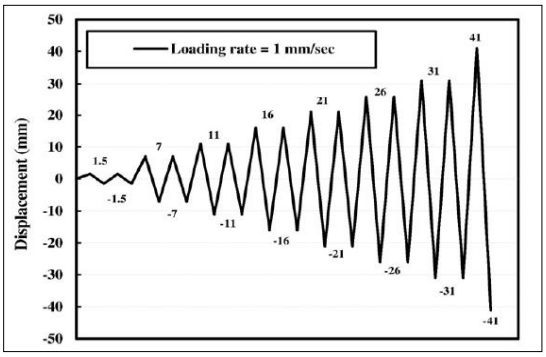

b. Loading protocol used by Amiri et al. [34].

Fig 2. General characteristics of the verification models.

Table 2. Geometrical dimensions of the models studied by Amiri et al. [34].

Specimen	h	b_1	h_0/b_1	b_2	t	h_0/t	$h_u=h_d$	r_1, r_2
S1	80	14	5	6.3	20	3.5	8	10, 5
S2	80	17.5	4	7.87	20	3.5	9	10, 5
S3	80	20	3.5	9	20	3.5	10	10, 5
S4	80	23.33	3	10.5	20	3.5	11	10, 5
S5	80	28	2.5	12.5	20	3.5	13	10, 5

Cyclic and pushover analysis were conducted to confirm the behavior of materials on the reconstructed sample S5. Results of cyclic, pushover analysis and deformation of this sample are shown in Figures 3-a to 3-e. Comparing the diagrams of cyclic and pushover with the results of the article by Amiri et al., shows that the behavior of materials and the constructed model in the cyclic analysis is in good consistency with results of the mentioned research. Also, equivalent strain distribution results from the

finite element analysis show a very similar failures mode compared to the laboratory specimen, as the removed paint on the experimental specimen represents places with higher strains, similar the green edges on the equivalent strain counters output from the finite element model (Figure 3-d and 3-e). For displacements larger than 50mm in pushover analysis, struts internal force is turned into pure tension and afterwards a tensional failure occurs. Since the purpose of Figure 3-c is demonstrating that the pushover curve covers cyclic graph, data for displacements larger than 50mm gives no additional information in this regard and thus was removed.

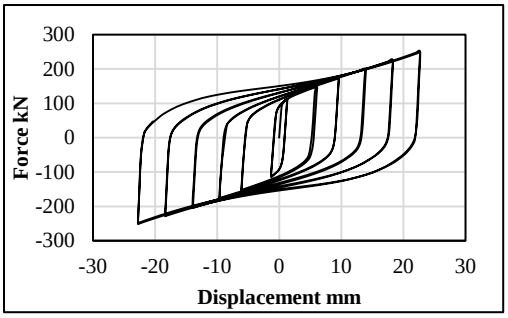

a. The diagram of the cyclic loading of the reconstructed model.

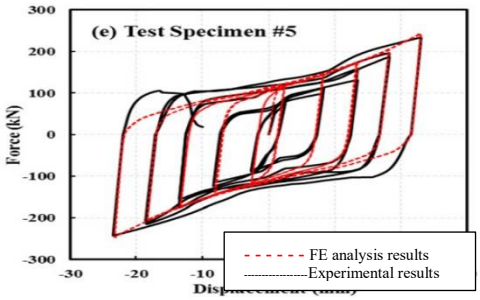

b. results of the research model of Amiri et al. [34].

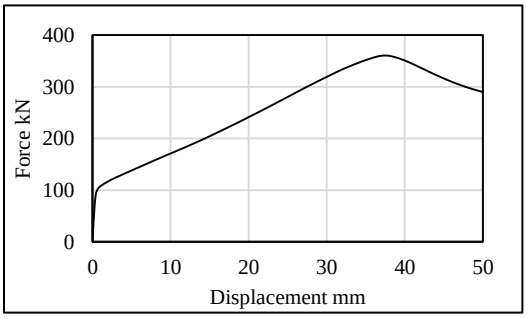

c. Force-displacement graph of the reconstructed model.

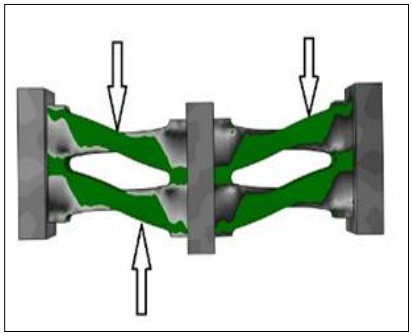

d. Deformation of the numerical model of the S5 sample.

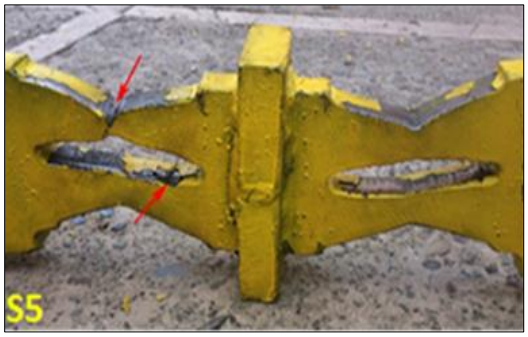

e. Deformation of laboratory model sample S5 [34].

Fig 3. Results of modeling verification.

3. Models Introduction and Analysis Method

3.1. Design Equations

Six types of Metallic Yielding Dampers, namely, Steel Plate Added Damping and Stiffness Elements (ADAS), Dual-Pipe Damper (DPD), Shear-and-Flexural Yielding Metallic Dampers (SAFYD), Steel Panel Damper (SPD), Steel Slit Damper (SSD) and Steel Shear Panel Dampers (SSPD) are simulated and analyzed, using ABAQUS finite element package. Figure 4 demonstrates general schematic geometry, shape and parameters of the aforementioned dampers.

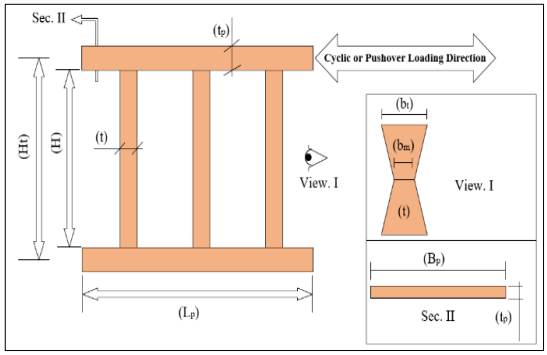

a. ADAS general geometry.

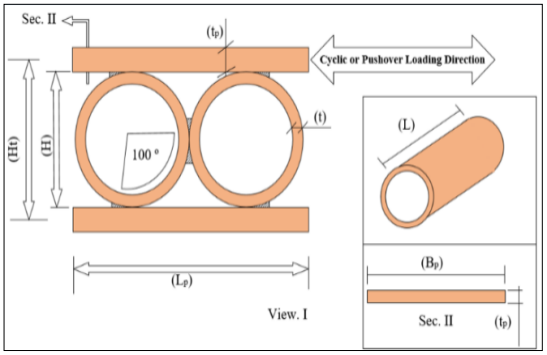

b. DPD general geometry.

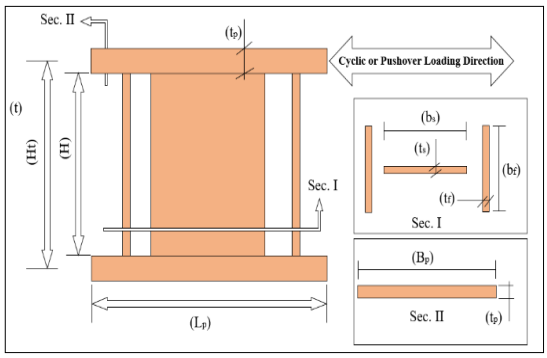

c. SAFYD general geometry.

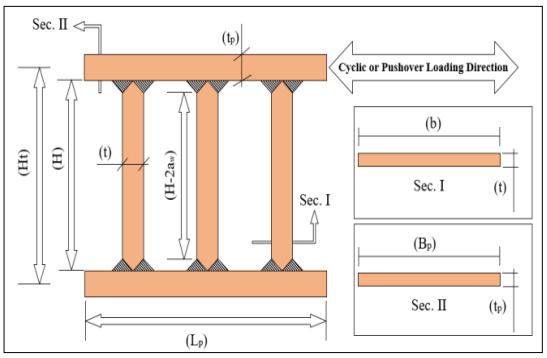

d. SPD general geometry.

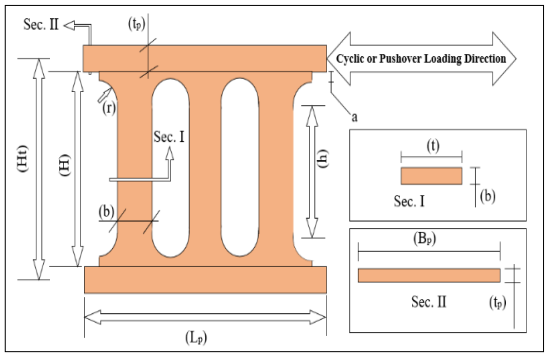

e. SSD general geometry.

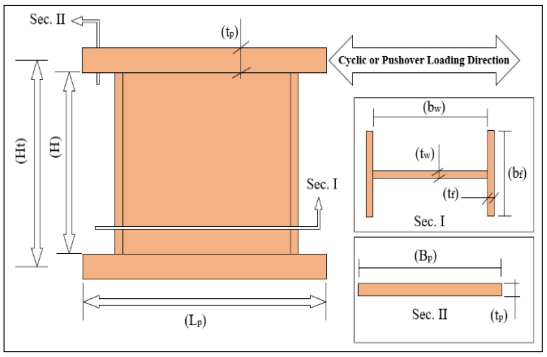

f. SSPD general geometry.

Fig 4. General geometrical characteristics and schematics of damper types.

The design equations of each damper type are presented separately in the following. The design equations of ADAS dampers are given out in Equations 1 and 2 [35,36]:

$$M_p = n[f_y bt^2 / 4] \quad (1)$$

$$V_p = 2n(M_p / H) = n[f_y bt^2 / 2H] \quad (2)$$

The design equations of DPD dampers are given out in Equations 3 to 5 [30]:

$$\Delta_y = 0.0001[4.75D - 8.2](D/t) \quad (3)$$

$$K_0 = 3156(L)(D/t)^{-3.14} \quad (4)$$

$$P_y = K_0 * \Delta_y \quad (5)$$

The design equations of SAFYD dampers are given out in Equations 6 to 8 [31]:

$$V_y = V_{ys} + V_{yf} \quad (6)$$

$$V_{ys} = (b_s t_s / 1.2)(f_y / \sqrt{3}) \quad (7)$$

$$V_{yf} = (b_f t_f^2 / 1.5H)(f_y) \quad (8)$$

The design equations of SPD dampers are given out in Equations 9 to 13:

$$H = H_t - t_p \quad (9)$$

$$H^* = H - 2a_w \quad (10)$$

$$Z = (bt^2)/4 \quad (11)$$

$$M_p = Zf_y \quad (12)$$

$$V_p = (nbt^2 f_y)/(2H) \quad (13)$$

The design equations of SSD dampers are given out in Equations 14 to 16 [1,6,15]:

$$H^* = h + 2r^2 / H_t \quad (14)$$

$$h = H - 2(a + r) \quad (15)$$

$$P_y = \min\left\{nf_y b^2 t / (2H^*), 2nf_y bt / 3\sqrt{3}\right\} \quad (16)$$

The design equations of SSPD dampers are given out in Equations 17 to 19 [32]:

$$V_y = (f_y / \sqrt{3})(t_w)(b_w + 2t_f) \quad (17)$$

$$K_d = (G/H)(t_w)(b_w + 2t_f) \quad (18)$$

$$U_p = V_y / K_d \quad (19)$$

Geometrical parameters in Equations 1 to 19, are demonstrated in Figure 4, in detail. Also, f_y is steel yield stress, P_y is equivalent force at yielding displacement, Δ_y is yielding displacement of the damper, V_y is total yielding capacity of the damper, V_{ys} is yielding shear force of damper struts, V_{yf} is yielding shear force of damper flange, V_p is plastic shear capacity of the struts section, M_p is plastic bending capacity of the struts section, n is number of struts, K_0 elastic stiffness of the damper, K_d is theoretical shear stiffness and U_p is yielding stage deformation. For each of the six damper types, three heights, namely 15, 21, 27cm are designed based on the design equations. Geometrical dimensions of all eighteen models are presented in Table 3.

Table 3. Geometrical dimensions of models.

Steel Plate Added Damping and Stiffness Element Models									
Model	H_t cm	H cm	b_t cm	b_m cm	t cm	L_p cm	B_p cm	t_p cm	N
ADAS15	15	13	6	2.3	1.5	18	10	2	4
ADAS21	21	19	8	2.3	1.1516	18	10	2	4
ADAS27	27	25	8	2.3	1.8	18	10	2	4
Dual-Pipe Damper Models									
Model	H_t cm	H=D cm	L cm	t cm	L_p cm	B_p cm	t_p cm	-	-
DPD15	15	13	8	0.894	26	10	2	-	-
DPD21	21	19	8	1.092	40	10	2	-	-
DPD27	27	25	8	1.262	50	10	2	-	-
Shear-and-Flexural Yielding Metallic Damper Models									
Model	H_t cm	H cm	b_f cm	t_f cm	b_s cm	t_s cm	L_p cm	B_p cm	t_p cm
SAFYD15	15	13	8	1.59	6	0.36	18	10	2
SAFYD21	21	19	8	1.93	6	0.36	18	10	2
SAFYD27	27	25	8	2.21	6	0.36	18	10	2
Steel Panel Damper Models									
Model	H_t cm	H cm	b cm	t cm	a_w cm	L_p cm	B_p cm	t_p cm	n
SPD15	15	13	8	1.19	1	18	10	2	4
SPD21	21	19	8	1.49	1	18	10	2	4
SPD27	27	25	8	1.73	1	18	10	2	4
Steel Slit Damper Models									
Model	H_t cm	H cm	b cm	t cm	a cm	r cm	L_p cm	B_p cm	t_p cm
SSD15	15	13	0.79	3	1.5	2	18	10	2
SSD21	21	19	1.44	3	1.5	2	18	10	2
SSD27	27	25	2.12	3	1.5	2	18	10	2
Steel Shear Panel Damper Models									
Model	H_t cm	H cm	b_f cm	t_f cm	b_w cm	t_w cm	L_p cm	B_p cm	t_p cm
SSPD15	15	13	8	0.3	12	0.3	18	10	2
SSPD21	21	19	8	0.3	12	0.3	18	10	2
SSPD27	27	25	8	0.3	12	0.3	18	10	2

3.2. Analysis Method and Mesh Size Convergence Analysis

Metallic Yielding Dampers are often installed at the plastic hinge formation locations which is either in braces or at both ends of the beams (Figure 5-a and 5-b). This placement of the damper in these parts of the structure leads to its optimal behavior, prevents damage to the main members, and also provides replacement circumstances of the damper in case of damage. As shown in Figure 5-c and 5-d, under the cyclic loading, the Metallic Yielding Dampers will be subjected to bending and shear. Therefore, for the purpose of optimizing the simulation process, structural models are reduced to the demonstrated state in Figure 5-d, which is a suitable structural model to study the behavior of dampers in both situations.

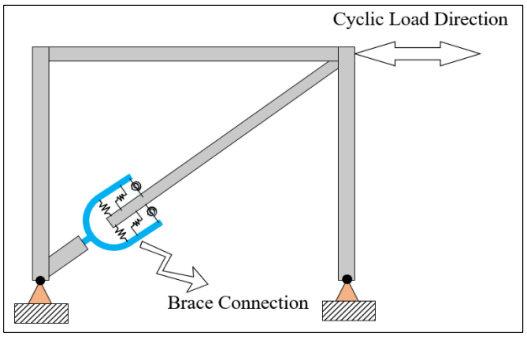

a. Metallic Yielding Dampers in bracing system.

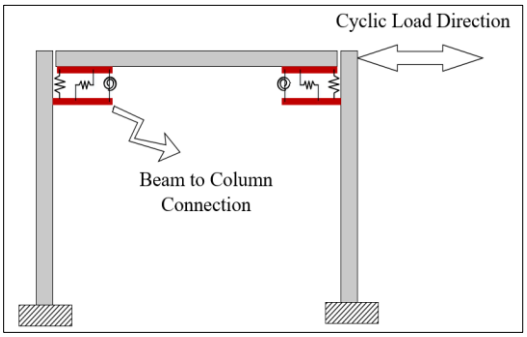

b. Metallic Yielding Dampers as beam to column connection.

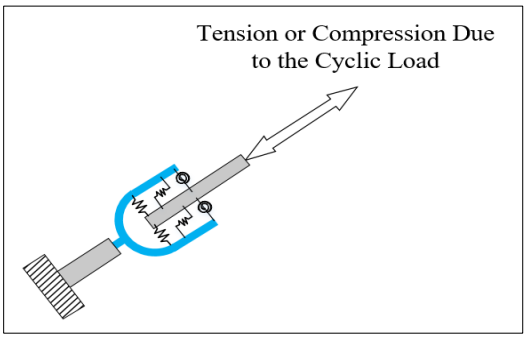

c. Schematics brace damper.

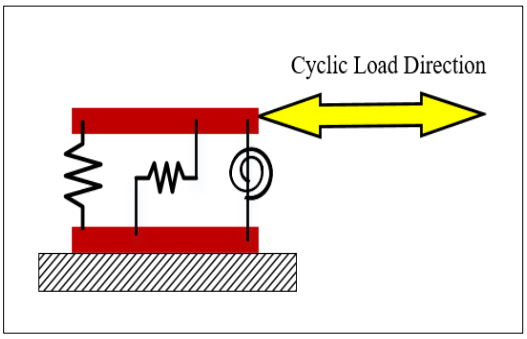

d. Schematics of beam to column connection damper.

Fig 5. Position of the Metallic Yielding Dampers in the structure.

In this research, the FEMA461 standard loading protocol [37], which is described in Table 4, is used for loading the models. Effective stiffness in each cycle of loading is shown by Keff, and effective damping in each cycle is shown by the Beff. These parameters are obtained from Equations 20 and 21 [38]. In these equations, |F+| and |F-| are the forces related to |Δ+| and |Δ-| which are maximum and minimum displacement in each loading cycle, respectively. Also, in Equation 21, Eloop is the dissipated energy in each cycle or the inner surface of the force-displacement graph in each cycle.

Table 4. Loading protocol based on FEMA461 [37].

Displacement (mm)	No. of Cycles
1.5	two Cycles
2.03	two Cycles
2.94	two Cycles
4.12	two Cycles
5.77	two Cycles
8.06	two Cycles
11.28	two Cycles
15.79	two Cycles
22.06	two Cycles
31.25	two Cycles

$$K_{eff} = (|F^+| + |F^-|)/(|\Delta^+| + |\Delta^-|) \quad (20)$$

$$B_{eff} = (2/\pi)[E_{loop}/K_{eff}(|\Delta^+| + |\Delta^-|)^2] \quad (21)$$

For all dampers except SSD, quadratic hexagonal elements and for SSD dampers, quadratic tet elements are used. To capture the flexure and shear effect, three and in some cases four layers of elements are used in thickness. Boundary conditions are set in accordance with Figure 5-d with the upper and lower flanges fixed in all directions except the loading direction in the upper flange. Loads are applied in accordance with Figure 5-d. In order to determine the suitable mesh size for all models Mesh Convergence Analysis is used. For instance, in SSD and SPD damper types, default mesh size proposed by the ABAQUS was reduced by one unit at each stage of the analysis, and for each stage pushover analysis was conducted. Results of these series of analyses are presented in Figure 6 and for explicit comparison, relative difference of both shear and bending to larger mesh size is given in Figure 7. The aforementioned results show that for meshing with a dimension of less than 4 mm, the changes in the SSD and SPD model results are less than 1 and 2%, respectively, which is very low.

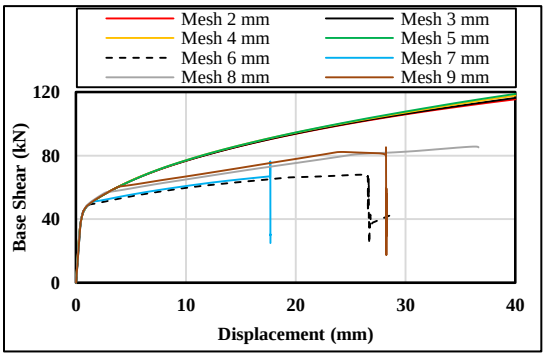

a. Pushover results of SSD model with the different mesh size.

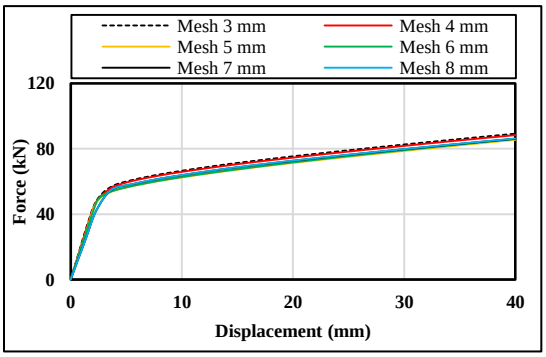

b. Pushover results of SPD model with the different mesh size.

Fig 6. Pushover results for mesh convergence.

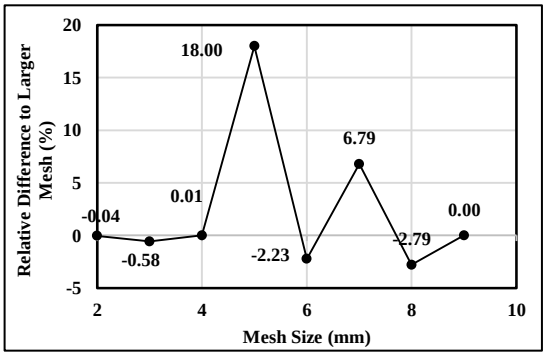

a. Relative difference of shear to larger mesh size in the SSD model.

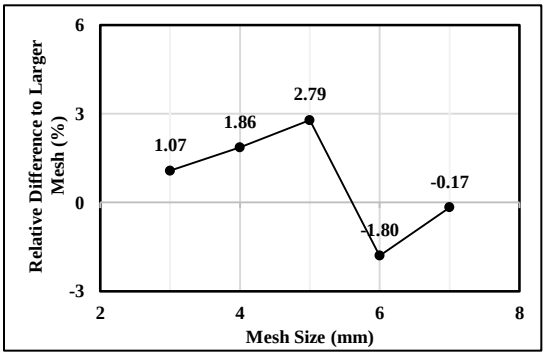

b. Relative difference of shear to mesh size in the SPD model.

Fig 7. Results of mesh convergence analysis.

4. Numerical Analysis Results

4.1. Cyclic and Pushover Analyses Graphs

Force-displacement graphs of the models with cyclic analysis are given in Figure 8. Based on these graphs, it can be concluded that loops created by the SPD type dampers are larger than other dampers, which indicates a higher level of energy dissipation in this type of damper. Also, when dampers height is increased, inner area of their cyclic diagrams which represents energy dissipation performance decreases.

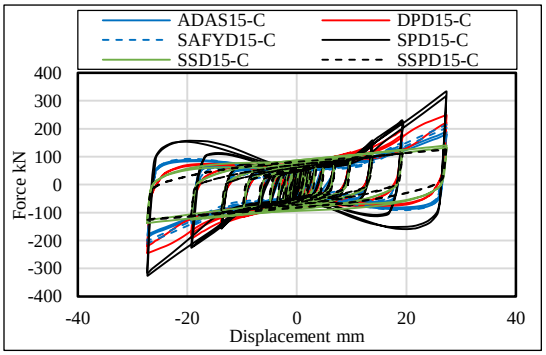

a. Cyclic diagram of the models with a height of 15 cm.

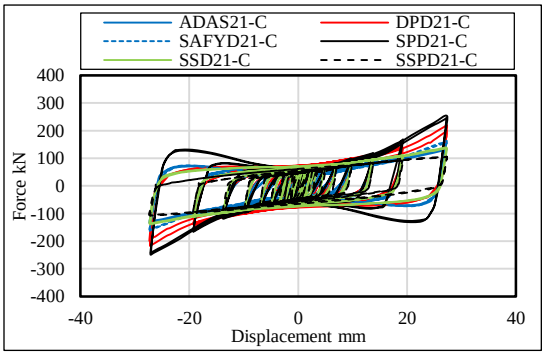

b. Cyclic diagram of the models with a height of 21 cm.

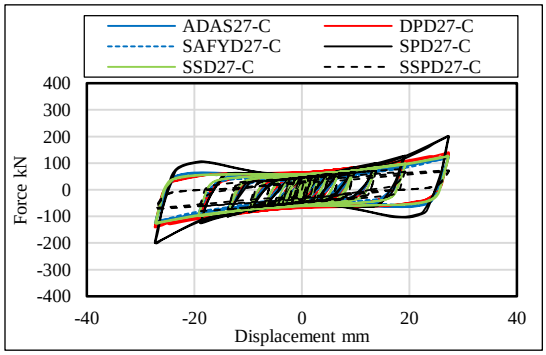

c. Cyclic diagram of the models with a height of 27 cm.

Fig 8. Cyclic analysis results.

All the simulated dampers were examined under a pushover load, results of which are shown in Figure 9. The 5 tons yield strength is conveniently observable in all diagrams of the dampers. Also, the issue of the reduction of the area under the force-displacement diagram in these diagrams confirms the results of cyclic loading. In all models of the dampers, the SPD type dampers have the highest area under the graph, which shows the suitable hyper-elastic behavior and energy dissipation. Meanwhile, the SSPD type dampers have higher initial stiffness than other dampers. However, their stiffness is severely reduced at the final stages of pushover loading. In contrast to all the other dampers, which have a monotone process, the DPD dampers get a decreased and increased slope in the hyper-elastic stage of the force-displacement diagram, which show different and almost unpredictable behavior of this type of damper in the forces beyond

its yield strength. Also, results show that this type of damper has the lowest internal shear, which is almost equal to zero and insignificant compared to other dampers. It is assumed that when applying rolling force to a pipe, perpendicular to its axis, almost half of the pipe will get pressured and the other half will be under tension. In a way this behavior is associated with the tensile performance of parts of the pipes under each cycle of loading and needs further investigation.

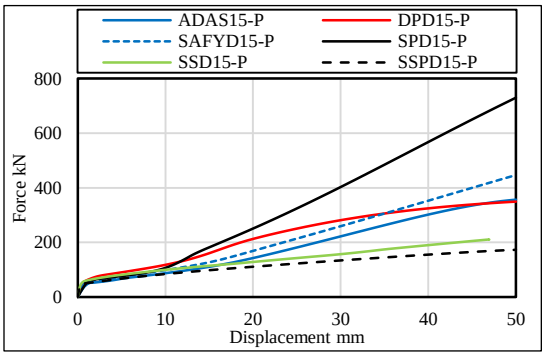

a. Pushover diagram of models with a height of 15 cm.

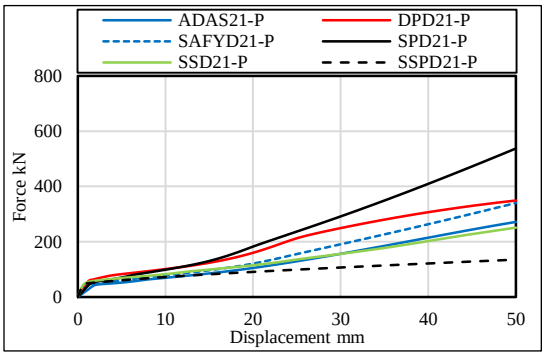

b. Pushover diagram of models with a height of 21 cm.

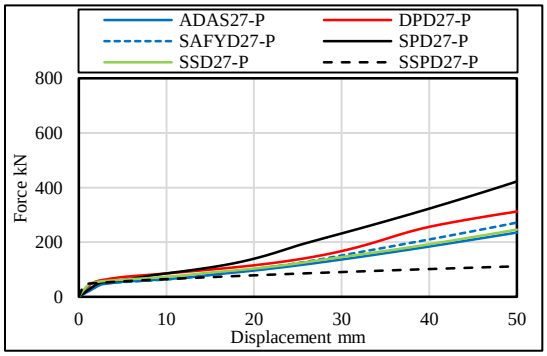

c. Pushover diagram of models with a height of 27 cm.

Fig 9. Pushover analysis results.

4.2. Effective Stiffness and Damping Comparison

Effective stiffness of the dampers is essentially the slope of the Force-Displacement graph (Figure 8) and is extracted based on Equation 20. Diagrams of the effective stiffness of the dampers are shown in Figure 10, which show that by increasing the height of steel dampers, their effective stiffness decreases. This was observed in the enlarged Force-Displacement graph (from Figure 8). In general, effective stiffness graphs become almost stable at the final stages of loading. DPD and ADAS types of dampers showed the highest and lowest effective stiffness in the initial loading cycles, respectively. But the significant point is that the effective stiffness curve of the SPD type damper has become horizontal around the 15th cycle onwards and even shows a slight increase, which brings its curve higher than the other dampers. This phenomenon indicates that this type of damper maintains

its coherence in long earthquakes and demonstrates a better function in respect to stiffness. Also, stability of the effective stiffness of this type of damper can be considered as a capability and advantage in respect of lifetime of the structure. Based on these observations, SPD and DPD types of dampers can be a good choice to create an effective stiffness suitable for buildings during an earthquake.

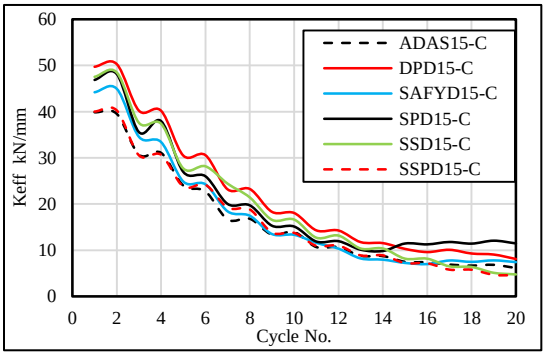

a. Effective stiffness diagram of models with a height of 15 cm.

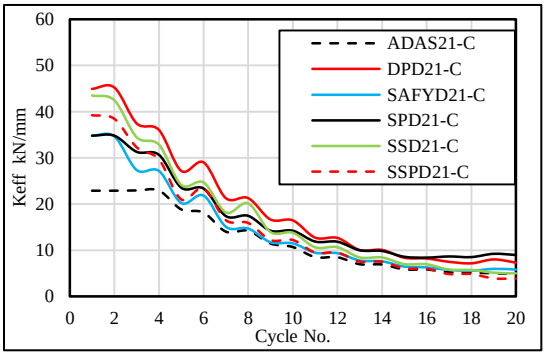

b. Effective stiffness diagram of models with a height of 21 cm.

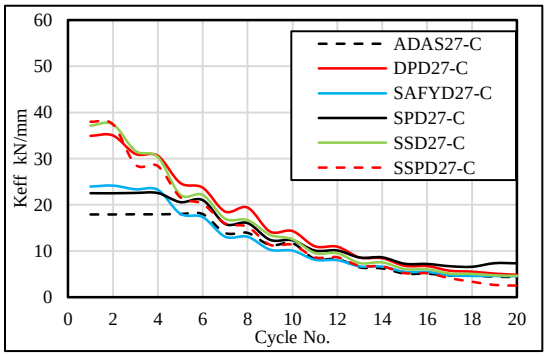

c. Effective stiffness diagram of models with a height of 27 cm.

Fig 10. Effective stiffness comparison.

Effective stiffness of the dampers is averaged during the whole cyclic analysis and the average effective stiffness of the dampers is shown in Figure 11. According to these diagrams, it can be concluded that DPD damper has the highest average effective stiffness and ADAS has the lowest.

Effective damping curve of the studied models for each cycle is extracted using Equation 21 and is shown in Figure 12-a. The mentioned diagram has a lot of fluctuations and not many direct deductions can be made from it. Also, as demonstrated in figure 12-b, energy dissipation of DPD and SPD dampers are higher than other dampers and it is the lowest for ADAS dampers. Furthermore, the average effective damping and accumulated effective damping parameters are derived for the loading period, which is shown in the Figures 13 and 14, respectively.

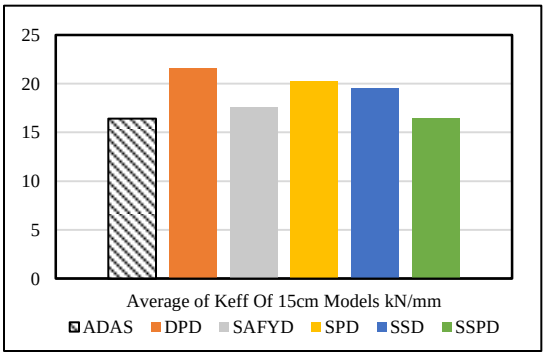

a. Average effective stiffness of models with a height of 15 cm.

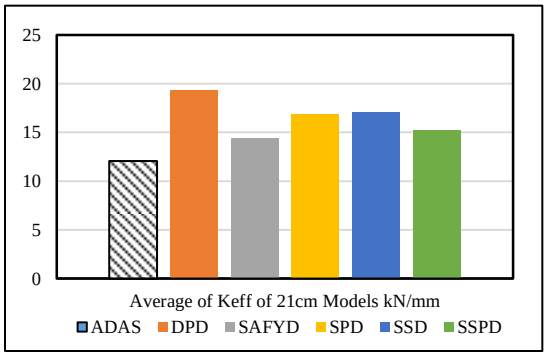

b. Average effective stiffness of models with a height of 21 cm.

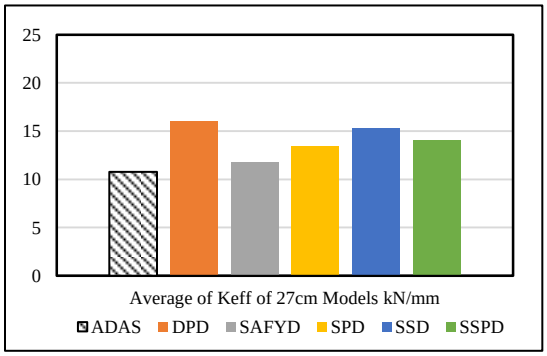

c. Average effective stiffness of models with a height of 27 cm.

Fig 11. Average effective stiffness comparison.

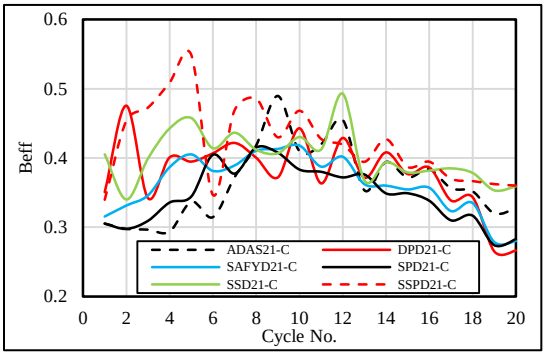

a. Effective damping.

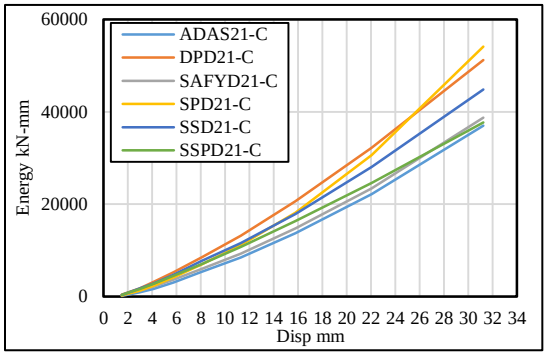

b. Energy dissipation.

Fig 12. Effective damping and energy dissipation of models with a height of 21 cm.

Based on these diagrams, compared to other dampers, SSPD and SSD damper types have the highest and lowest average effective damping, respectively. Standard deviation of the average damping of SSD damper with a height of 15 cm with a value of 0.028 has the lowest amount among all dampers, which indicates more stability of the effective damping rate during the loading process in this type of damper. As the height increases,

average effective damping of the dampers also decreases, which, like the effective stiffness, indicates that in the process of designing dampers, for achieving higher stiffness and damping, a minimum height should be considered. Based on these observations, implementation of SSD damper is a suitable choice to achieve a certain amount of damping in a building. Also, accumulated damping diagram indicates that the overall damping performance during an earthquake stays almost stable in one type of damper with increasing the height. Among the studied models, SSPD and SSD dampers have the two highest accumulated damping.

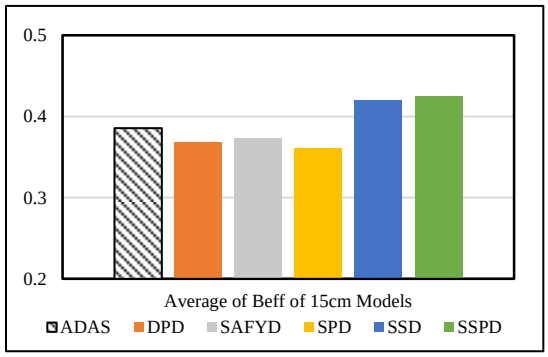

a. Average effective damping of models with a height of 15 cm.

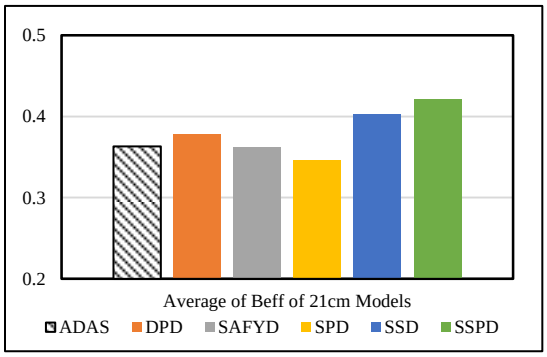

b. Average effective damping of models with a height of 21 cm.

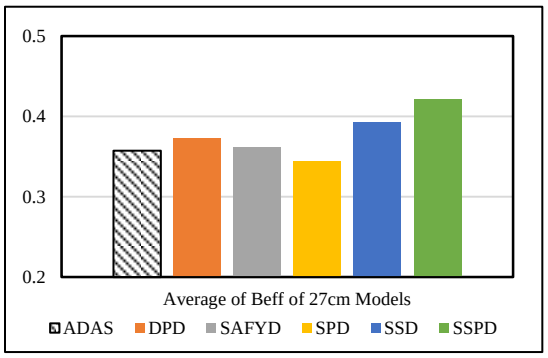

c. Average effective damping of models with a height of 27 cm.

Fig 13. Average effective damping comparison.

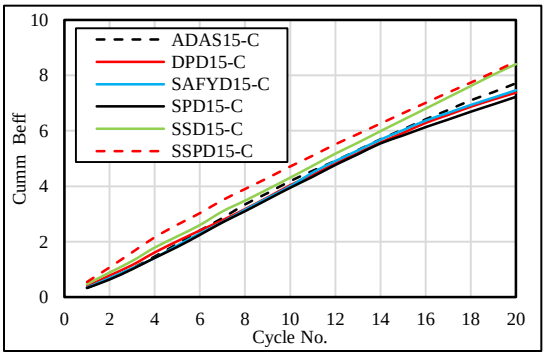

a. Accumulated effective damping for models with height of 15cm.

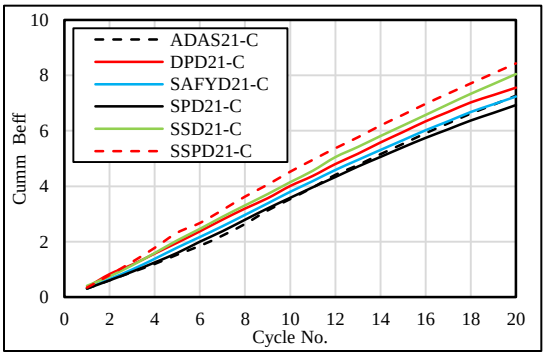

b. Accumulated effective damping for models with height of 21cm.

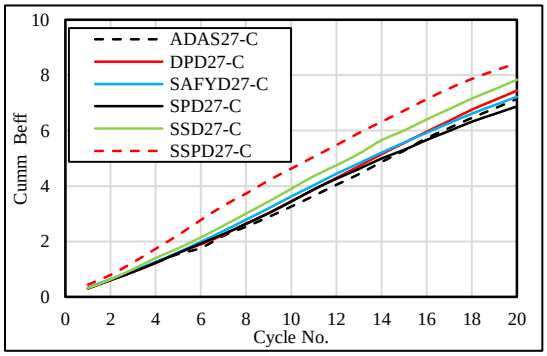

c. Accumulated effective damping for models with height of 27cm.

Fig 14. Accumulated effective damping.

4.3. Internal Forces of Dampers

In the next step, shear force and bending moment of the constituent members of dampers were extracted and investigated. Based on the extracted maximum shear force and bending moment of the dampers, which are shown in Figures 15 and 16, it can be concluded that by increasing the height, dampers behavior leans towards flexural behavior. The SPD type dampers have the highest shear force, and SSD type dampers have the highest bending moment among all dampers. However, considering the DPD model, it becomes clear that this type of damper has the lowest internal shear and flexure, which are insignificant compared to other dampers and almost equal to zero. This issue can be explained based on the suitable deformation of this type of damper, and its tolerance against forces resulting from displacement in the form of tensile in the central arc. Deformation and equivalent strain distribution of all dampers is shown in Figure 17.

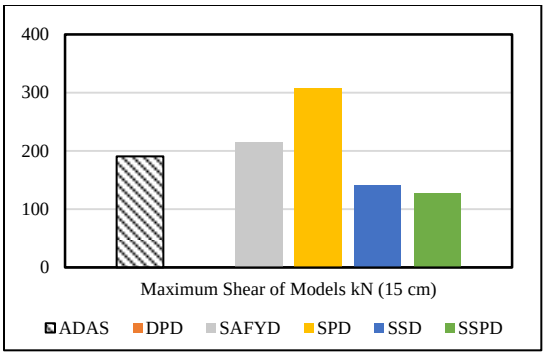

a. Maximum shear force of models with a height of 15 cm.

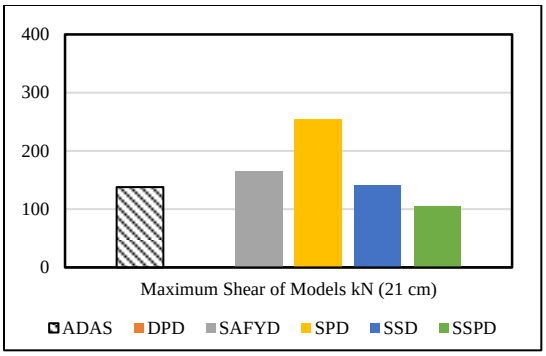

b. Maximum shear force of models with a height of 21 cm.

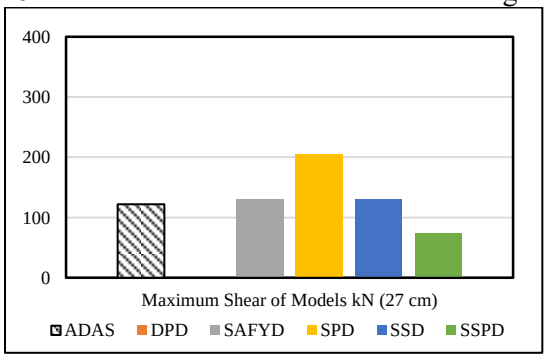

c. Maximum shear force of models with a height of 27 cm.

Fig 15. Maximum internal shear force.

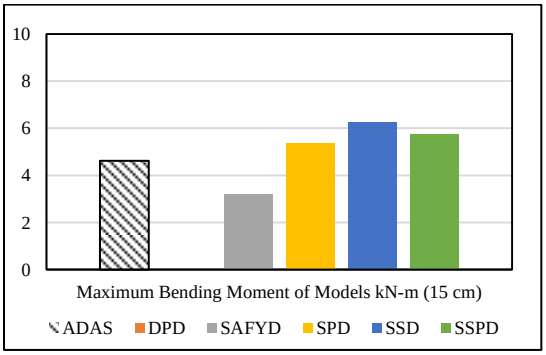

a. Maximum flexural force of models with a height of 15 cm.

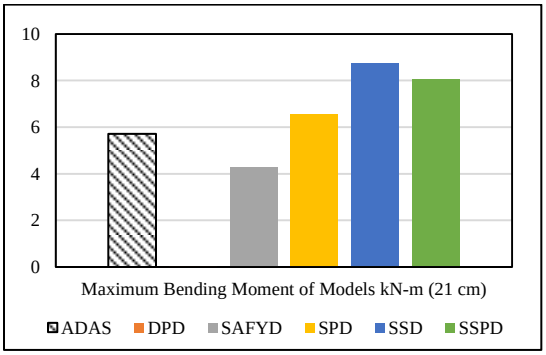

b. Maximum flexural force of models with a height of 21 cm

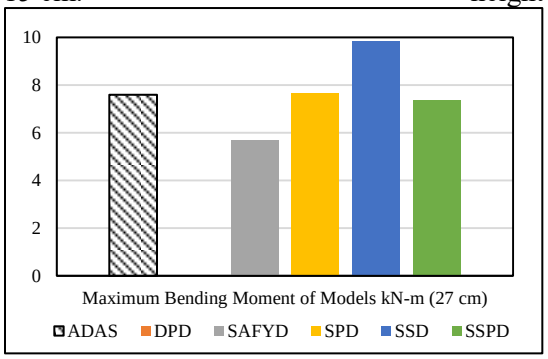

c. Maximum flexural force of models with a height of 27 cm.

Fig 16. Maximum internal bending moment.

Behavior of steel under tensile is more predictable than its behavior under bending and shear and as Figure 15 and 16 indicate, DPDs behavior is mainly tensile based. Therefore, the DPD type damper with elliptical deformation is mainly affected by the tensile force. In contrast to this, other dampers behavior is mainly dominated by shear, bending and buckling rupture of the dampers struts which makes their behavior more unpredictable. Therefore, behavior of DPD damper can be attributed to its suitable configuration compared to other dampers. At the same time, in cases of SSD, SAYYD, and SSPD dampers local buckling was observed in the studied models (Figure 17), which seems to be the source of weaker behavior of these dampers.

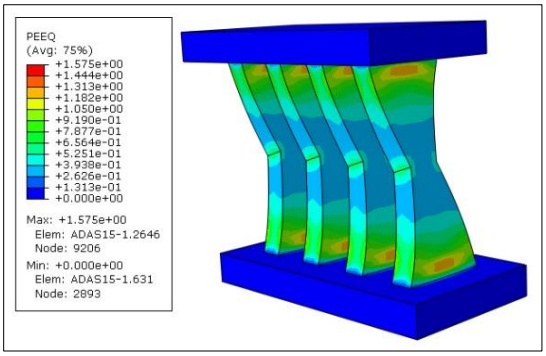

a. Deformation and yield points of ADAS damper.

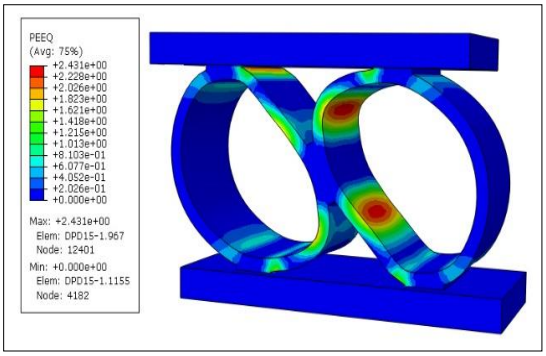

b. Deformation and yield points of DPD damper.

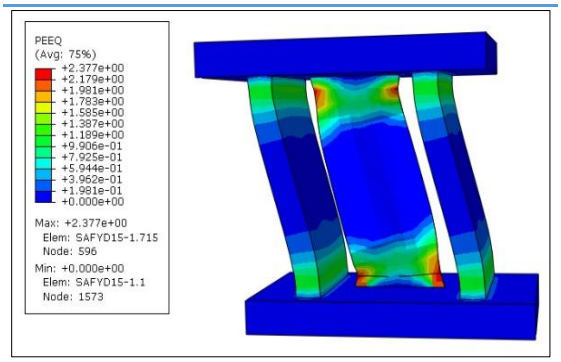

c. Deformation and yield points of SAFYD damper.

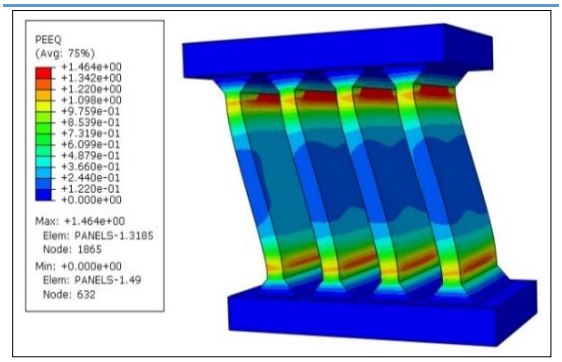

d. Deformation and yield points of SPD damper.

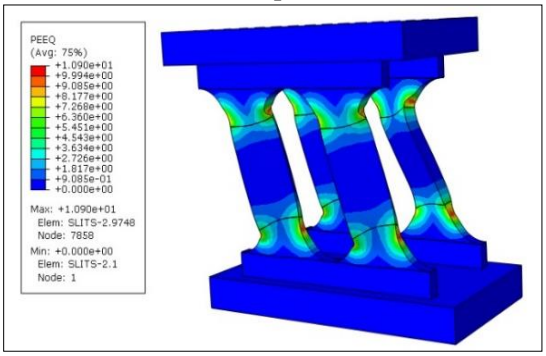

e. Deformation and yield points of SSD damper.

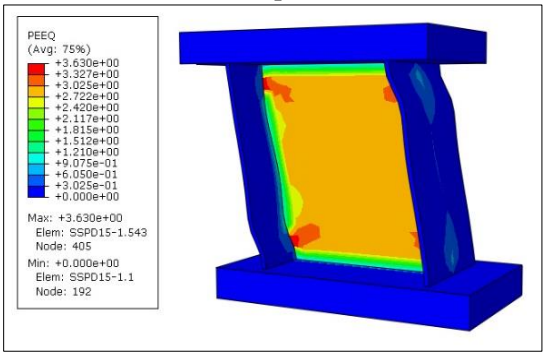

f. Deformation and yield points of SSPD damper.

Fig 17. Deformation and yield points of dampers.

5. Conclusion

According to the findings of this research, the following results can be presented:

- According to the cyclic diagram of dampers, SPD and DPD dampers have a higher energy dissipation level than other dampers.

- In the pushover analysis, the 5 tons yield strength was observable in all dampers, which indicates the relatively high accuracy of the dampers design equations.

- In the pushover analysis, SPD damper has the highest response to uniform displacement among dampers, which indicates its high stiffness and energy dissipation compared to other dampers.

- As the height of the dampers increases, their effective stiffness and damping is reduced.

- Compared to other dampers, the SSPD and SPD dampers have the highest and lowest average effective damping, respectively.

- SSD damper with a height of 15 cm shows the most stable effective damping. Also, among the studied models, SSPD and SSD dampers have the highest cumulative damping.

- As the height of the dampers increases, shear behavior decreases, and flexural behavior becomes more dominant.

- In the SSD, SSPD, and SAFYD dampers, the issue of flange buckling is the main weakness.

- DPD and ADAS dampers show the highest and lowest effective stiffness, respectively.

- SPD dampers show an increase in effective stiffness at the last stages of loading, which indicates its suitable behavior and performance in long earthquakes.

- SPD and DPD dampers have a higher energy dissipation level than other dampers.

- SPD damper has the highest response to uniform displacement among dampers, which indicates its high stiffness and energy dissipation compared to other dampers

- DPD damper resists the forces imposed on it, in the form of a tensile with a suitable deformation, which is a more ductile and as such, it has a more predictable behavior compared to other dampers.

- Based on the last five points, SPD and DPD dampers are good choices to reach a target effective stiffness for a building during an earthquake.

- In general, it seems possible to reach the demanded stiffness, damping, and cohesion of the damper in the loading process by using SPD and DPD dampers. Also, the main advantage of these dampers is their suitable behavior at lower heights, which mitigates the buckling problem, and at the same time has the least protrusion from the ceiling and visibility in the architectural space.

References

[1] Saffari H, Hedayat AA, Nejad MP. Post-Northridge connections with slit dampers to enhance strength and ductility. J Constr Steel Res 2013;80:138–52. https://doi.org/10.1016/j.jcsr.2012.09.023.

[2] CEN. Euro code 8: Design of Structures for Earthquake Resistance. Part 1: General rules, seismic actions and rules for buildings 2009.

[3] Miller DK. Lessons learned from the Northridge earthquake. Eng Struct 1998;20:249–60.

https://doi.org/10.1016/S0141-0296(97)00031-X.

[4] Nakashima M, Inoue K, Tada M. Classification of damage to steel buildings observed in the 1995 Hyogoken-Nanbu earthquake. Eng Struct 1998;20:271–81. https://doi.org/10.1016/S0141-0296(97)00019-9.

[5]. Rezaee Manesh, M., Fattahi, S., & Saffari, H. Investigation of Earthquake Significant Duration on the Seismic Performance of Adjacent Steel Structures in Near-Source. Journal of Rehabilitation in Civil Engineering 2020, 9(1), 84–101. https://doi.org/10.22075/jrce.2020.20373.1410.

[6] Oh S-H, Kim Y-J, Ryu H-S. Seismic performance of steel structures with slit dampers. Eng Struct 2009;31:1997–2008. https://doi.org/10.1016/j.engstruct.2009.03.003.

[7] Federal Emergency Management Agency (FEMA), Recommended Seismic Design Criteria for New Steel Moment-Frame Buildings, FEMA350, Washington (DC) 2000.

[8] Chen C-C, Lee J-M, Lin M-C. Behaviour of steel moment connections with a single flange rib. Eng Struct 2003;25:1419–28. https://doi.org/10.1016/S0141-0296(03)00104-4.

[9] Gorji Azandariani M. Gorji Azandariani A, Abdolmaleki H. Cyclic behavior of an energy dissipation system with steel dual-ring dampers (SDRDs). Journal of Constructional Steel Research 2020; 172 https://doi.org/10.1016/j.jcsr.2020.106145

[10] Rousta A-M, Shojaeifar A, Gorji Azandariani M, Saberiun A, Abdolmaleki H. Cyclic behavior of an energy dissipation semi-rigid moment steel frames (SMRF) system with LYP steel curved dampers. Structural Engineering and Mechanics; 2021; 80; 129-142; https://doi.org/10.12989/sem.2021.80.2.129

[11] Lee C-H, Ju YK, Min J-K, Lho S-H, Kim S-D. Non-uniform steel strip dampers subjected to cyclic loadings. Eng Struct 2015;99:192–204. https://doi.org/10.1016/j.engstruct.2015.04.052.

[12] Oh SH. Seismic Design of Energy Dissipating Multi-Story Frame with Flexible-Stiff Mixed Type Connection, Ph.D. Thesis, Japan, Tokyo University. 1998.

[13] Chan RWK, Albermani F. Experimental study of steel slit damper for passive energy dissipation. Eng Struct 2008;30:1058–66. https://doi.org/10.1016/j.engstruct.2007.07.005.

[14] Zheng J, Li A, Guo T. Analytical and experimental study on mild steel dampers with non-uniform vertical slits. Earthq Eng Eng Vib 2015;14:111–23. https://doi.org/10.1007/s11803-015-0010-9.

[15] Köken A, Köroğlu MA. Experimental Study on Beam-to-Column Connections of Steel Frame Structures with Steel Slit Dampers. J Perform Constr Facil 2015; 29: 04014066. https://doi.org/10.1061/(ASCE)CF.1943-5509.0000553.

[16] Chen S-J, Jhang C. Experimental study of low-yield-point steel plate shear wall under in-plane load. J Constr Steel Res 2011;67:977–85. https://doi.org/10.1016/j.jcsr.2011.01.011.

[17] Gorji Azandariani M, Gorji Azandariani A, Abdolmaleki H. Numerical and analytical investigation of cyclic behavior of steel ring dampers (SRDs). Journal of Thin-Walled Structures 2020; 151; https://doi.org/10.1016/j.tws.2020.106751

[18] Mohammadi M, Kafi M-A, Kheyroddin A, Ronagh H-R. Experimental and numerical investigation of an innovative buckling-restrained fuse under cyclic loading. Journal of Structures 2019; 22;186-199; https://doi.org/10.1016/j.istruc.2019.07.014

[19] Gorji Azandariani M, Mohammad Ali Kafi M-A, Gholhaki M. Innovative hybrid linked-column steel plate shear wall (HLCS) system: Numerical and analytical approaches. Journal of Building Engineering; 2021; 43; https://doi.org/10.1016/j.jobe.2021.102844

[20] Gorji Azandariani M, Rousta A-M, Usefvand E, Abdolmaleki H, Improved seismic behavior and performance of energy-absorbing systems constructed with steel rings. Journal of Structures; 2021; 29; 534-548; https://doi.org/10.1016/j.istruc.2020.11.041

[21] Rousta A-M, Gorji Azandariani M. Micro-finite element and analytical investigations of seismic dampers with steel ring plates. Steel and Composite Structures, 2022; 43; 5, 565-579; https://doi.org/10.12989/scs.2022.43.5.565

[22] Usefvand M, Rousta A-M, Azandariani M-G, Abdolmaleki H. Steel dual-ring dampers: Micro-finite element modelling and validation of cyclic behavior. Smart Structures and Systems, 2021; 28; 579; https://doi.org/10.12989/SSS.2021.28.4.579

[23] Rousta A-M, Zahrai S.M. Parametric study of a proposed hybrid damping system : KE + VLB in Chevron braced frames. Acta Technica; 2018; Vil. 63-4B, 1–16.

[24] Ali Mohammad Rousta and Seyed Mehdi Zahrai. Cyclic testing of innovative two-level control system: Knee brace & vertical link in series in chevron braced steel frames. Structural Engineering and Mechanics. 2017; Vol. 64-3; 301-310; https://doi.org/10.12989/sem.2017.64.3.301

[25] Gupta VV, Reddy G, Pendhari SS. Performance-Based Design of RC Structures Subjected to Seismic Load Using a Hybrid Retrofitting Method with Friction Damper and Steel Bracing. Comput Eng Phys Model 2022;5:19–35. https://doi.org/10.22115/cepm.2022.317119.1191.

[26] Ma X, Borchers E, Pena A, Krawinkler H, Billington S, Deierlein GG. Design and behavior of steel shear plates with openings as energy-dissipating fuses. John A Blume Earthq Eng Cent Tech Report, (173) 2010.

[27] Tagawa H, Yamanishi T, Takaki A, Chan RWK. Cyclic behavior of seesaw energy dissipation system with steel slit dampers. J Constr Steel Res 2016;117:24–34. https://doi.org/10.1016/j.jcsr.2015.09.014.

[28] Lee C-H, Kim J, Kim D-H, Ryu J, Ju YK. Numerical and experimental analysis of combined behavior of shear-type friction damper and non-uniform strip damper for multi-level seismic protection. Eng Struct 2016;114:75–92. https://doi.org/10.1016/j.engstruct.2016.02.007.

[29] Houshmand-Sarvestania, A, Totonchi A, Shahmohammadi M-A, Salehipour H. Numerical assessment of the effects of ADAS yielding metallic dampers on the structural behavior of steel shear walls (SSWs), Mechanics Based Design of Structures and Machines. 2020; ; https://doi.org/10.1080/15397734.2021.1875328

[30] Maleki S, Mahjoubi S. Dual-pipe damper. J Constr Steel Res 2013;85:81–91. https://doi.org/10.1016/j.jcsr.2013.03.004.

[31] Sahoo DR, Singhal T, Taraithia SS, Saini A. Cyclic behavior of shear-and-flexural

yielding metallic dampers. J Constr Steel Res 2015;114:247–57. https://doi.org/10.1016/j.jcsr.2015.08.006.

[32] Xu L-Y, Nie X, Fan J-S. Cyclic behaviour of low-yield-point steel shear panel dampers. Eng Struct 2016;126:391–404. https://doi.org/10.1016/j.engstruct.2016.08.002.

[33] ABAQUS 2017. ABAQUS user's manual. Simulia

[34] Ahmadie Amiri H, Najafabadi EP, Estekanchi HE. Experimental and analytical study of Block Slit Damper. J Constr Steel Res 2018;141:167–78. https://doi.org/10.1016/j.jcsr.2017.11.006.

[35] Li H-N, Li G. Experimental study of structure with "dual function" metallic dampers. Eng Struct 2007;29:1917–28. https://doi.org/10.1016/j.engstruct.2006.10.007.

[36] Whittaker A, Bertero V, Alonso J, Thompson C. Earthquake Simulator Testing of Steel Plate Added Damping and Stiffness Elements 1988. https://doi.org/10.13140/RG.2.1.1455.3207.

[37] FEMA 461. Interim Testing Protocols for Determining the Seismic Performance Characteristics of Structural and Nonstructural Components, Washington, D.C., June 2007 n.d.

[38] Minimum Design Loads and Associated Criteria for Buildings and Other Structures. Reston, VA: American Society of Civil Engineers; 2017. https://doi.org/10.1061/9780784414248.